# Combined influence of hydrodynamics and chemotaxis in the distribution of microorganisms around spherical nutrient sources

Nikhil Desai and Arezoo M. Ardekani*
*School of Mechanical Engineering, Purdue University, West Lafayette, Indiana 47907, USA*

(Received 25 February 2018; revised manuscript received 15 May 2018; published 31 July 2018; corrected 27 August 2018)

We study how the interaction between hydrodynamics and chemotaxis affects the colonization of nutrient sources by microorganisms. We use an individual-based model and perform probabilistic simulations to ascertain the impact of important environmental and motility characteristics on the spatial distribution of microorganisms around a spherical nutrient source. In general, we unveil four distinct regimes based on the distribution of the microorganisms: (i) strong surface colonization, (ii) rotary-diffusion-induced "off-surface" accumulation, (iii) a depletion zone in the spatial distribution, and (iv) no appreciable aggregation, with their occurrence being contingent on the relative strengths of hydrodynamic and chemotactic effects. More specifically, we show that the extent of surface colonization first increases, then reaches a plateau, and finally decreases as the nutrient availability is increased. We also show that surface colonization reduces monotonically as the mean run length of the chemotactic microorganisms increases. Our study provides insight into the interplay of two important mechanisms governing microorganism behavior near nutrient sources, isolates each of their effects, and thus offers greater predictability of this nontrivial phenomenon.

DOI: 10.1103/PhysRevE.98.012419

## I. INTRODUCTION

Chemotaxis can be defined as the ability of bacteria to perceive gradients in ambient nutrient or chemical concentrations and adjust their motility so as to "climb" up or down these gradients. It is one of the most widely studied properties of bacteria, particularly for the enteric bacterium *E. coli* [1–4]. The nutrient/chemical responsible for chemotaxis is called the chemoeffector. The motion of *E. coli* is termed "run and tumble" because it consists of almost straight runs separated by sudden tumbles, i.e., abrupt changes in the swimming direction [1–4]. Bacteria rely on temporal comparison of ambient nutrient concentrations to gauge chemoeffector gradients and refine their motion as required [5–9]. Based on the feedback, a variety of changes can take place to alter bacterial motion, e.g., a change in swimming speed as a function of ambient concentration (chemokinesis), a change in the frequency of tumbling, or even a shift in the regime of swimming from run and tumble to "run reverse and flick" [10]. The cumulative effect of the above sequence of actions is to prolong the bacterium's stay in any desired region. For example, chemokinesis can either slow bacteria down in regions of high nutrient concentration or it can speed them up so as to have proportionately faster gradient climbing. Similarly, bacteria are known to increase their average exposure to nutrients and thus fulfill their energetic requirements by tumbling (or reversing) less often in nutrient hotspots. In addition to chemotaxis—which is an active response by a bacterium to ambient physicochemical stimuli—a bacterium's motility can also get altered passively via hydrodynamic interactions (HI) with nearby boundaries [11]. Some examples are "swimming on the right-hand side" [12], swimming in circles [13–17], reversal of swimming direction [18], and wall attraction and accumulation [19–26]. These near-surface phenomena, coupled with bacterial chemotaxis, are of utmost importance in the comprehension of biofilm formation and evolution [27–29]. While studies focusing solely on HI [12–26], on chemotaxis without HI [30–38], or on chemotaxis and HI due to self-generated bacterial flows in infinite domains [39,40] abound; the combined effect of chemotaxis and HI on the locomotion of microorganisms near a boundary that is also a source of a chemoattractant has not been studied. The studies that do consider the effects of fluid flow on bacterial motion (chemotactic or otherwise) near surfaces have been mostly limited to the cases where the bacterial cell is translated and rotated by a pre-existing background flow [31–36]. In absence of any background flows, a consistent description of HIs should involve fluid flow that is generated on account of bacterial swimming and its proximity to surfaces.

In this paper, we aim to understand the combined or competitive effects of hydrodynamic and chemotactic attraction of model microorganisms to spherical nutrient sources. We study the motion of a bacterium that can run and tumble near a stationary, spherical surface which acts as a source of the chemoeffector. Therefore, the motion is dictated by three different mechanisms: (i) translation due to inherent motility as well as hydrodynamic interaction (attraction) with the nutrient source (which can be a rigid sphere or a drop), (ii) rotation due to hydrodynamic interaction and random effects like thermal and athermal diffusion, and (iii) chemotactic reorientation due to the spatial distribution of a chemoeffector having a prescribed concentration on the surface of the source [30].

The fluid flow far from a bacterium can be modeled as that due to a force dipole, i.e., two equal and opposite, collinear forces with an infinitesimal separation between them [24].

*ardekani@purdue.edu

 

A force dipole that lies within a few (1–3) body lengths from the surface of a rigid sphere (which, in an experiment, can be a colloid [41] or an isolated nutrient source like a marine snow particle) is prone to getting hydrodynamically trapped onto the surface of the sphere [25,26]. Beyond this separation, hydrodynamics alone cannot lead to attachment of microorganisms onto nutrient sources. In fact, Drescher *et al.* performed experiments and concluded that hydrodynamics becomes important only when a bacterium reaches within a few microns from a surface and that hydrodynamic interactions successfully explain the long residence times of *E. coli* near no-slip surfaces [42]. This means that in order for hydrodynamics-based capture to occur, a bacterium must reach within an $\lambda O(1)$ body length from the spherical surface. This initial approach could either be a chance encounter or directed motion in the form of chemotaxis. It is this idea that motivates our study to understand how effective chemotaxis is, in conjunction with hydrodynamics, in the capture of microorganisms around a spherical nutrient source with prescribed surface concentration of the chemoattractant.

A study of this type has been carried out in the past by Jackson [30], but without accounting for any hydrodynamic interactions. Another related work is by Bearon [35], where they quantify the rate at which motile bacteria colonize sinking aggregates like marine snow, phytoplankton, etc. [38]. This study neglects HIs and considers the effect of the background flow (generated due to a sphere settling at zero Reynolds number [43]) on the bacterium's position and orientation but does not consider biased tumbling due to chemotaxis. In a similar fashion, Locsei and Pedley [36] studied the motion of a bacterium tracking an alga wherein they evaluate a background flow field due to a model algal cell. They then use this flow to translate and rotate the bacterial cell and neglect other HIs between the algal and the bacterial cell. In addition, they model chemotaxis in an empirical fashion based on experimental observations [44], where the chemotactic reorientation involves just a reversal in the swimming direction whenever the separation between the algal and bacterial cells exceeds a threshold.

In this paper, we wish to provide a mathematical model that consistently accounts for chemotaxis and hydrodynamic interactions, in situations where no other background flow exists. To this goal, it is essential to include (i) chemotactic bias in bacterial motion stemming from the temporal comparison of nutrient concentrations by a bacterium, and, (ii) the fluid flow (and concomitant bacterial motion) that stems solely from the interaction between the bacterium and the surface or boundary. Our objective is to obtain the spatial distribution (in the form of a probability distribution function, or, pdf) of noninteracting chemotactic microorganisms released at a given separation from the (nutrient) source and with an arbitrary initial orientation. This pdf will, in general, be a function of (i) hydrodynamic parameters like the size (diameter) of the source, the swimming speed of the microorganism, and the thrust force it exerts on the fluid, i.e., its dipole strength and (ii) chemotactic parameters like the chemoeffector concentration on the surface of the source and the tumbling frequency of the microorganism. A thorough understanding of these functional dependencies is warranted to successfully isolate the effects of chemotaxis from those of hydrodynamics; and in the process, better understand the dynamics of microorganism locomotion and colonization in the context of lab-on-a-chip setups or marine ecosystems.

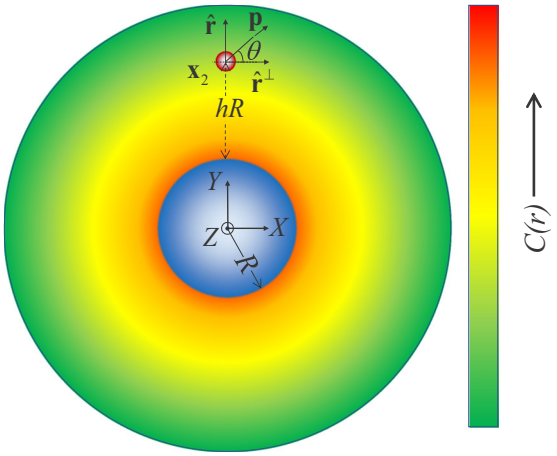


FIG. 1. A schematic of the problem being solved, showing a spherical nutrient source of radius $R$, a spherical swimming microorganism of radius $b$ oriented along the unit vector $\mathbf{p}$, and the spherically symmetric chemoattractant distribution around it $C(r)$. The origin of a fixed coordinate system $XYZ$ lies at the center of the source. The coordinate system defined by the unit vectors $\hat{\mathbf{r}}$, $\hat{\mathbf{r}}^{\perp}$ and $\hat{\mathbf{r}}^{\perp}\times\hat{\mathbf{r}}$ can rotate and translate with respect to the fixed coordinate system, as the microorganism moves through the fluid. In a quiescent, unbounded fluid ($h\to\infty$), the microorganism will swim along the direction $\mathbf{p}$. The hydrodynamic-interaction-induced translational velocity, $\mathbf{u}_{HI}$, and rotational velocity, $\mathbf{\Omega}_{HI}$, of the microorganism are expressed as functions of its separation from the surface $h$, and its in-plane orientation $\theta$ [see Eqs. (4) and (5)]. Note that $h$ is the dimensionless separation of the microorganism from the source.

The rest of the paper is organized as follows. We first describe the governing equations of fluid flow and the boundary conditions on the surface of a rigid, stationary sphere (which, in our case, represents the source of chemoattractant). This enables us to discuss the hydrodynamics-induced locomotion of the model microorganism. We then describe the randomness in the microorganism motion, the chemoattractant distribution, and the modeling of run-and-tumble chemotaxis for a single microorganism. We also comment on the near-field effects and how they are expected to alter our model. Once the mathematical model is laid out, we present the results of the probabilistic simulations for the translational and rotational dynamics of the microorganism. In all cases, we perform relevant comparative studies and discussion of the results to pinpoint the influence of different parameters involved. Finally, we end by making some concluding remarks.

## II. MATHEMATICAL MODELING AND METHODOLOGY

### A. Hydrodynamic interaction

The contribution of the microorganism to the fluid flow is modeled as a pusher force dipole (dipole strength $F$ oriented along $\mathbf{p}$; see Fig. 1). Even though the force dipole representation is most accurate when the flow field is being analyzed far away from the microorganism, we note that such representations have been shown to be accurate at distances

as small as a few body lengths away from rigid walls [19,24] and interfaces [45,46]. These have also been used to study the locomotion and hydrodynamic trapping of microswimmers around rigid spherical obstacles [25] and spherical drops [26]. To model the bacterial motion in the unbounded case (when it is far away from any surface), we make two additions: (i) We allow the force dipole to have swimming velocity $V_s\mathbf{p}$ in an unbounded fluid, where $V_s$ is the swimming speed of the microorganism, and (ii) we assume that in an unbounded fluid, the dipole orientation can tumble with a characteristic tumbling frequency $\tau_0^{-1}$ and diffuse over the unit sphere with a (rotary) diffusivity $D_r$; this part is discussed in detail in Sec. II B.

The effect of a solid boundary near the bacterium, i.e., the hydrodynamic interaction (HI), is incorporated by first solving the governing equations for fluid flow with appropriate boundary conditions. These include the differential forms of the conservation of mass,

$$\nabla \cdot \mathbf{v} = 0, \tag{1}$$

and momentum,

$$-\nabla P + \mu \nabla^2 \mathbf{v} = -F\,(\mathbf{p}\cdot\nabla)\{\mathbf{p}\cdot\boldsymbol{\delta}(\mathbf{x}-\mathbf{x}_2)\}, \tag{2}$$

in the Stokes flow regime, because for the length scales involved in our problem, the flow inertia is negligible. Equations (1) and (2) need to be solved subject to the boundary conditions:

$$\mathbf{v}(|\mathbf{x}| = R) = 0,$$
$$\mathbf{v}(|\mathbf{x}| \to \infty) = 0. \tag{3}$$

In the above equations, $\mathbf{v}$, $P$, and $\mu$ are the fluid's velocity, pressure, and dynamic viscosity, respectively. $R$ is the radius of the spherical nutrient source. $\mathbf{x}$ is the position at which the velocity needs to be evaluated, $\mathbf{x}_2$ is the position vector from the origin of the coordinate system to the center of the microorganism (see Fig. 1), and $\boldsymbol{\delta}(\mathbf{x})$ is the three-dimensional Dirac $\delta$ function. Equations (1)–(3) can be solved for $\mathbf{v}(\mathbf{x})$ and $P(\mathbf{x})$, by using the method of images as shown in Ref. [47]. Thereafter, an application of the Faxen's law for a sphere, by treating the image flow field as an ambient flow and utilizing the force-free and torque-free conditions, yields the linear ($\mathbf{u}_{HI}$) and angular ($\boldsymbol{\Omega}_{HI}$) velocity of the force dipole, due to the hydrodynamic influence of the nearby particle (see Refs. [25,26]):

$$\frac{\mathbf{u}_{HI}}{V_s} = -\frac{3A\alpha_D(1-3\sin^2\theta)(A+h)}{2h^2(2A+h)^2}\hat{\mathbf{r}} + \frac{3A^3\alpha_D(2A^2+6Ah+3h^2)\sin 2\theta}{4h^2(2A+h)^2(A+h)^3}\hat{\mathbf{r}}^{\perp}, \tag{4}$$

$$\frac{\boldsymbol{\Omega}_{HI}}{V_s/b} = -\frac{3A^3\alpha_D(2A^2+6Ah+3h^2)\sin 2\theta}{4h^3(2A+h)^3(A+h)^2}(\hat{\mathbf{r}}^{\perp}\times\hat{\mathbf{r}}). \tag{5}$$

In Eqs. (4) and (5), $b$ is a measure of the microorganism size (if assumed to be spherical, then $b$ is its radius), $h = (|\mathbf{x}_2| - R)/b$ is the dimensionless separation of the microorganism from the surface of the source, $A = R/b$ is the dimensionless radius of the source, $\theta$ is the in-plane orientation of the microorganism (see Fig. 1), and $\alpha_D = F/(8\pi\mu b^2 V_s)$ is the dimensionless dipole strength of the microorganism. Before proceeding, we make an important note regarding the generality of the hydrodynamic aspect of our study. Equations (4) and (5) describe the swimming dynamics of a model microorganism near a rigid spherical nutrient source. It is also possible to derive the same for motion around spherical drops by using appropriate boundary conditions in place of (3), as done by Shaik and Ardekani [48]. In this study, we restrict ourselves to the analysis of motion around rigid, spherical nutrient sources (e.g., marine snow particles). However, a similar analysis can be performed for a nutrient source like an oil drop (i.e., for a spherical fluid-fluid interface); for details see Ref. [26] and the appendix. For a viscosity ratio corresponding to crude oil, there is only a minor quantitative change in the final results of interest (see Fig. 12 in the appendix). Therefore, we note that our study also reflects the accumulation trends around crude oil drops that are the sole source of carbon for a wide class of marine bacteria [49]. Thus, the results of this study can be used to understand bioremediation in an oil spill.

Once $\mathbf{u}_{HI}$ and $\boldsymbol{\Omega}_{HI}$ are known, the motion of the microorganism can be defined in terms of the evolution equations for its position $\mathbf{x}_2(t)$ and orientation $\mathbf{p}(t)$, where $t$ is the time. The former is given by

$$\frac{d\mathbf{x}_2}{dt} = \mathbf{u}_{HI} + V_s\mathbf{p}, \tag{6}$$

while the *hydrodynamic component* of the latter is

$$\left.\frac{d\mathbf{p}}{dt}\right|_{\text{hydrodynamic}} = \boldsymbol{\Omega}_{HI}\times\mathbf{p}. \tag{7}$$

Equation (7) is not complete yet because we have not accounted for two important randomness effects in the motion of any bacterium: the run-and-tumble motion and thermal or athermal diffusion. We now turn our attention to modeling these effects.

### B. Chemotactic reorientation

The motion of a bacterium in an unbounded, quiescent fluid is characterized by run and tumble, i.e., nearly straight swimming (runs) interspersed with abrupt reorientations (tumbles) due to certain flagellar mechanisms [50–52]. The runs themselves are not perfectly straight due to various reasons (Brownian rotation, flagellar imperfections, ATP availability) and the bacterium is seen to undergo rotary diffusion during the course of each run [53]. In this section, we discuss the incorporation and implementation of these reorientations into our model. The rotary diffusion is straightforward and just adds a random component to the right-hand side of Eq. (7); written as a stochastic differential equation, this yields

$$\mathbf{p}_{n+1} = \mathbf{p}_n + \Delta t(\boldsymbol{\Omega}_{HI})_n\times\mathbf{p}_n + \sqrt{4D_r\Delta t}\,\boldsymbol{\eta}_r\times\mathbf{p}_n, \tag{8}$$

where $D_r$ is the rotary diffusivity of the bacterium and $\boldsymbol{\eta}_r$ is the Gaussian white noise on the unit sphere [3,53,54], the subscripts $n$ and $n+1$ refer to the values of the variables at the current, and the next time step, respectively. In general, the rotary diffusivity is obtained by using the Stokes-Einstein relations along with the mobility matrices of the system under consideration [11]. Because of the changing geometry of the problem, the mobility matrices will be a function of the

position and the orientation of the microorganism, and the effect of Brownian rotation will be a more involved stochastic differential equation (see Refs. [55,56] for details) instead of Eq. (8). Also, the magnitude of the fluctuations will be a function of the microorganism's distance from the source. For the sake of simplicity, however, we assume the mobility matrix to be constant and isotropic, in which case Eq. (8) holds. We emphasize that this does not alter the essential physics that we observe in our study. We discuss this idea in detail in the appendix. The tumbling of the bacterial cell is a probabilistic event, modeled as a Poisson process with rate $\tau_0^{-1}$ [3]. This means that in an unbounded fluid, the probability of a tumble to occur after an infinitesimal interval $dt$ is constant and is given by

$$P_{t,0} = dt/\tau_0. \tag{9}$$

Therefore, $1/\tau_0$ is the mean tumbling frequency for a bacterium, and a tumble is effected by the following rule [57,58]:

$$\begin{aligned} \mathbf{p}_{n+1} &= \phi \mathbf{p}_n + (1-\phi)\mathbf{p}', \\ \phi &\equiv H(\Re_{n+1} - P_{t,0}), \end{aligned} \tag{10}$$

where $H$ is the Heaviside function [59], and $\Re_{n+1}$ is a random number chosen from a uniform distribution on [0, 1]. Therefore, during a run (if $P_{t,0} < \Re_{n+1}$), the bacterium reorients smoothly via Eq. (8), but in case of a tumble (if $P_{t,0} > \Re_{n+1}$) it changes its orientation instantaneously to a new orientation $\mathbf{p}'$. This post-tumble orientation could either be one from a uniform distribution on the unit sphere (an isotropic tumble) or it could be biased, i.e., correlated in some way to the pretumble orientation (anisotropic tumble). In this study, we use a probability distribution $g(\beta)$ of the angle $\beta$ between the pre- and post-tumble orientations which has been observed experimentally for the bacterium *E. coli* [1], and a succinct mathematical expression is provided in Ref. [60]: $g(\beta) = (1 + \cos\beta)/2$. Note that in reality a tumble is not instantaneous (it takes around 0.1 s), but we assume it to be so for the current work.

The run and tumble described thus far enables a bacterium to perform a random walk through its environment, just like Brownian or diffusive motion. The effective diffusivity of this random walk is given by $D_{eff} = V_s^2\tau_0/3$ [61]. The true utility of this motility feature, however, is observed when a bacterium forages for nutrients. An intricate mechanism [22,52] allows the bacterium to alter its tumbling frequency—or equivalently, its run time—in such a way that it spends more (resp. less) time in a desired (resp. undesired) region, e.g., in a region that is rich (resp. poor) in nutrients. As a result, the rate of the Poisson process (or, equivalently, the tumbling frequency) is no longer a constant $\tau_0^{-1}$, but it changes depending on the nutrient exposure of the bacterium. If the organism finds itself in regions of progressively increasing nutrient concentration, then its tumbling frequency reduces ($\tau > \tau_0$); and if the organism moves to regions of declining nutrient concentrations, then the tumbling frequency stays unaltered at $\tau = \tau_0$. It is therefore imperative to have an idea about the nutrient distribution, before proceeding on to model bacterial chemotaxis. The concentration $C$ of the nutrient or chemoeffector is governed by the following conservation equation,

$$\frac{\partial C}{\partial t} + \nabla \cdot (C\mathbf{v}) = D_C \nabla^2 C, \tag{11}$$

subject to the boundary conditions:

$$\begin{aligned} C(|\mathbf{x}| = R) &= C_0, \\ C(|\mathbf{x}| \to \infty) &= 0. \end{aligned} \tag{12}$$

$D_C$ in Eq. (11) is the nutrient diffusivity. We now proceed to make two simplifications to Eq. (11). First, we consider steady-state nutrient distribution, thus dropping the first term on the left-hand side of Eq. (11). Next, we note that the characteristic Peclet number for the problem is very small, which allows us to neglect the advection terms in Eq. (11). The Peclet number is

$$\mathrm{Pe} = \frac{V_s l_{\mathrm{ref}}}{D_C}, \tag{13}$$

where $V_s \approx 10$ $\mu$m/s is the reference velocity scale (the bacterium's swimming speed) and $l_{\mathrm{ref}}$ is a reference length scale (for phytoplankton, $l_{\mathrm{ref}} \approx 10$ $\mu$m; for oil drops, $l_{\mathrm{ref}} \approx$ 20–60 $\mu$m [62–64]). The value of $D_C$ for some typical nutrients—like $C_6$ sugar or hydrocarbons like $CH_4$—is $\approx 10^{-5}$ cm$^2$/s [65,66]. For the above-mentioned parameters, we see that the Pe is $O(0.1)$, and thus advection can be neglected as a first approximation. As a result, we obtain the very simple diffusion equation for the chemoeffector concentration,

$$D_C \nabla^2 C = 0, \tag{14}$$

which can be solved using the boundary conditions (12) to get

$$C(r) = \frac{C_0 R}{r}, \tag{15}$$

where $r = |\mathbf{x}_2|$ is the radial distance from the origin of the coordinate system (see Fig. 1). We can now define the chemotactic motion of the bacterium by relating its tumbling frequency to the temporal evolution of the nutrient concentration $C$ in the bacterial reference frame. To this end, we employ the biphasic tumbling frequency model developed by Brown and Berg for *E. coli* [2], but without the memory effect, i.e.,

$$\tau = \begin{cases} \tau_0 \exp\left[\alpha_C \frac{K_D}{(K_D+C)^2} \frac{DC}{Dt}\right], & \frac{DC}{Dt} > 0, \\ \tau_0, & \frac{DC}{Dt} \leqslant 0, \end{cases} \tag{16}$$

where $K_D$ is a measure of how well the chemoattractant binds to the chemoreceptor and $\alpha_C$ is a timescale characteristic to the system being studied. A lack of the memory effect means that $\tau$ depends only on the *instantaneous* rate of change (material derivative) of $C$ (i.e., $DC/Dt$) with respect to the bacterial motion, and not on the averaged time history of nutrient concentration [67]. It is clear that if the material derivative is positive, then the run time $\tau > \tau_0$; if the material derivative is negative, then the run time does not change, as observed in experiments with *E. coli* [2]. Equation (16) thus provides us with a framework that explains how tumbles assist a microorganism in foraging for desired chemical species. As the organism swims through its environment, it senses the changes in the ambient nutrient concentration and alters its tumbling statistics according to Eq. (16) [68,69]. Therefore, in the presence of a chemoeffector, a tumble occurs within

TABLE I. Summary of various mechanisms dictating swimming behavior near a rigid, spherical surface exuding a chemoattractant with a specified concentration at the surface of the source.

| Mechanism: dimensionless parameter | Contribution |
|---|---|
| Hydrodynamic interaction (HI): $\alpha_D$ and $A$ | Attraction of nearby microorganisms leading to scattering or trapping |
| Chemotaxis: $C_0/K_D$ and $\tau^*$ | Initial attraction of distant bacteria toward the nutrient source |
| Hard-core repulsion: $\lvert\mathbf{x}_2\rvert/(R+b) \leqslant 1$ | Balance with HI leads to orbiting or entrapment |
| Rotary diffusion: $D$ | Orientational fluctuations may cause the microorganism to escape from surface |

an infinitesimal time interval $dt$, if $P_t = dt/\tau > \Re_{n+1}$; notice how $P_t$ can be lesser than $P_{t,0}$ [Eq. (9)] if a chemoeffector is involved. We note that although the above model was developed for the enteric *E. coli*, a judicious choice of the quantity $\alpha_C$ and slight changes in the type of reorientation can enable us to mimic chemotactic responses that are not of the run-and-tumble type; e.g., see the recent work by Son *et al.* [70].

### C. Near-wall effects

So far, we have described the effect of HI and chemotaxis on the locomotion of a microorganism modeled as a force dipole. These descriptions are apt in situations when the microorganism is a few (>2) body lengths away from the source. What happens when the microorganism drifts to within two body lengths from the solid surface? In such a scenario, the far-field force dipole assumption can lead to the microorganism penetrating into the solid surface, an occurrence which is clearly aphysical. This could be prevented by (i) the inclusion of higher order singularities (and images) in Eq. (2) or (ii) use of the lubrication or thin-film approximation, as the microorganism-surface distance becomes very small. Both these methods are unwieldy, and so, for the sake of simplicity, we model the near-field hydrodynamics as a hard-core repulsion [20,21,25]; i.e., we set the normal velocity of the microorganism to be zero if its distance becomes less than one body length from the surface:

$$\frac{d\mathbf{x}_2}{dt} = \begin{cases} \mathbf{u}_{HI} + V_s\mathbf{p}; & |\mathbf{x}_2| \leqslant (R+b), \quad (\mathbf{u}_{HI} + V_s\mathbf{p})\cdot\hat{\mathbf{r}} > 0 \\ (\mathbf{u}_{HI} + V_s\mathbf{p})\cdot\hat{\mathbf{r}}^{\perp}; & |\mathbf{x}_2| \leqslant (R+b), \quad (\mathbf{u}_{HI} + V_s\mathbf{p})\cdot\hat{\mathbf{r}} \leqslant 0 \end{cases}. \tag{17}$$

While the evolution of the microorganism position $\mathbf{x}_2$ is clear from the relation (17), we still need to ascertain the evolution of the microorganism orientation $\mathbf{p}$, when it is close to the surface. The microorganism orientation is affected deterministically by $\boldsymbol{\Omega}_{HI}$ and randomly via the Gaussian white-noise (rotary diffusion, $D_r$) and the Poisson process [tumbling, Eq. (10)]. It is the third behavior that we need to treat carefully, keeping in mind how surfaces affect bacterial tumbling. As stated by Elgeti *et al.* in a recent review article, "the swimming behavior of bacteria close to surfaces differs from the run-and-tumble motion in free solution" [53]. This difference in swimming behavior is well documented in prior experimental studies [12–15,22,71]. Specifically, it is known that tumbling of the bacterium *E. coli* is reduced by as much as ≈50% in the proximity of solid surfaces [22,71] and that *E. coli* can escape these surfaces not by tumbling away but by diffusing their orientation away from the surface and then swimming away [20,21]. Even in the event that a tumble does occur, the post-tumble orientations are mostly restricted to the tangent plane at the location of the bacterium. The near-interface behavior of marine bacteria—that do not necessarily utilize the run-and-tumble motion of *E. coli*—has not been investigated in detail. Therefore, we take an empirical approach to near-surface tumbling and postulate that the microorganism ceases to tumble at distances from the solid surface that are less than twice its body length. The rotary diffusion of a bacterium, on the other hand, is independent of its ability to tumble or display other motility traits [3]. It is a well-known behavior of most bacterial species, both enteric and marine, and is attributed to thermal fluctuations and/or intrinsic irregularities. Therefore, the $D_r$ term influences the orientation $\mathbf{p}$ of the microorganism irrespective of its distance from the surface. In summary, the microorganism motion in the bulk (>2 body lengths separation) is governed by Eqs. (6), (8), (10), (15), and (16); while that near the surface (<2 body lengths separation) is governed by (8) and (17). In what follows, we numerically solve these equations for sufficiently large number of instances, to get statistically meaningful results and deduce the effect of the various mechanisms (see Table I) on the distribution of microorganisms around spherical nutrient sources.

## III. RESULTS AND DISCUSSION

### A. Interplay between hydrodynamic interaction and chemotaxis

We select the following scales to nondimensionalize the various quantities of interest: lengths by the characteristic microorganism size $b$ (1 $\mu$m), speeds by the swimming speed $V_s$ (10 $\mu$m/s), time by $b/V_s$ (0.1 s), dipole strength by $\mu b^2 V_s$ (0.01 pN $\mu$m), nutrient concentration by $K_D$, and rotary diffusivity by $V_s/b$ (10 $s^{-1}$). This yields the important dimensionless parameters, along with their orders of magnitude, in our study to be as follows: radius of the source $A = R/b \approx 20$–$60$, dipole strength $\alpha_D = F/(8\pi\mu b^2 V_s) \approx 0.1$–$2.0$ ($F \approx 0.1$–$10$ pN $\mu$m), diffusivity $D = D_r b/V_s \approx 10^{-5}$–$10^{-3}$, surface concentration (representative nutrient availability) $C_0/K_D \approx 10^{-2}$–$10^{2}$, and run time (or equivalently, inverse of tumbling frequency) $\tau^* = \tau_0 V_s/b \approx 4$–$12$.

In our simulations, the baseline parameters are: $\alpha_C = 300$ s, $C_0/K_D = 1.0$, $\tau^* = 6$, $\alpha_D = 0.8$ or $10^{-3}$, $A = 20$, $D =$

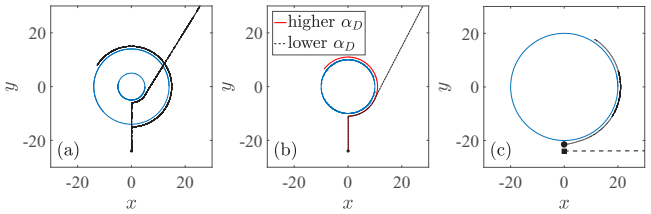


FIG. 2. (a) The concept of the critical trapping radius [25]: The swimmer trajectory around the smaller sphere escapes, while that around the larger sphere (whose radius is greater than a critical trapping radius) gets trapped. The swimmers' initial orientation, $\mathbf{p}(0) = \mathbf{e}_Y$. (b) Alternatively, for a fixed radius, only the swimmer with $\alpha_D$ larger than a critical dipole strength will get trapped around the sphere. (c) The concept of the basin of attraction [25]: The swimmer whose initial location is marked by a circle (resp. square) and whose trajectory is shown by a solid line (resp. by a dashed line), starts inside (resp. outside) the basin of hydrodynamic attraction, and thus it gets trapped onto (resp. escapes) the surface. The swimmers' initial orientation, $\mathbf{p}(0) = \mathbf{e}_X$. It is important to note that the basin of attraction is defined only in cases when hydrodynamic trapping is ensured.

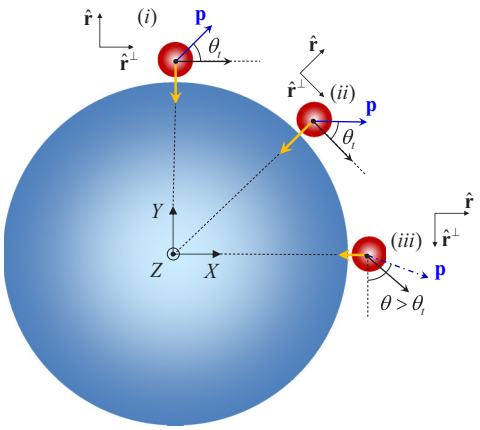


FIG. 3. An illustration of the effect of hydrodynamics on the motion of the microorganism as it gets trapped onto the surface of the nutrient source. The thin blue arrows are the microorganism's intrinsic motility $V_s\mathbf{p}$, the thick orange arrows are the hydrodynamic component of microorganism motion toward the center of the nutrient ($\mathbf{u}_{HI} \cdot \hat{\mathbf{r}}$), and the black arrows are the instantaneous velocity, $d\mathbf{x}_2/dt$ [Eq. (17)]. [(i), (ii)] Hydrodynamics—if strong enough—rotates the microorganism such that it always maintains a constant separation $h_t(\approx 1)$ and in-plane angle $\theta_t$, and such that $(\mathbf{u}_{HI} + V_s\mathbf{p}) \cdot \hat{\mathbf{r}} \leqslant 0$. As a result, the microorganism moves tangentially along the surface and stays trapped. (iii) Rotary diffusion—if significant—can cause the microorganism to rotate to an in-plane angle greater than $\theta_t$ which reduces the hydrodynamic attraction, causes $(\mathbf{u}_{HI} + V_s\mathbf{p}) \cdot \hat{\mathbf{r}} > 0$, and thus leads to escape.

$7.5\times10^{-4}$ (or, $D \approx 0$, when rotary diffusion is neglected). The swimming dynamics is solved for 10 000 instances, each running up to 200 dimensionless time units ($t_{\text{end}} = 200$). In each case, the initial position of the microorganism is 20 body lengths away from the source ($|\mathbf{x}_2(0)| = 40$), and the initial orientation is randomly assigned. The final result that we investigate is the distribution of the microorganisms' locations $r(=|\mathbf{x}_2|)$ at the end of the simulations. We compute two different quantities of interest: (i) a surface concentration $C_s$ and (ii) a radial distribution function $f(r)$. $C_s$ is the fraction of the total microorganisms that get trapped at the surface, i.e., those whose trajectory end point lies within a separation of 1.5 body lengths from the source. It is a measure of the surface colonization by the bacteria. $f(r)$ is a distribution function such that the fraction of microorganisms that lie in a thin spherical shell of radius $dr$ is equal to $4\pi r^2 f(r)dr$. In other words, the probability of finding a microorganism between $r$ and $r + dr$ is proportional to $4\pi r^2 f(r)dr$. $f(r)$ is normalized such that together with $C_s$, it satisfies

$$C_s + \int_{r=A}^{\infty} 4\pi r^2 f(r)dr = 1. \tag{18}$$

A confluence of chemotaxis, hydrodynamics, hard-core repulsion, and rotational diffusion shapes the behavior and subsequent distribution of the swimming microorganisms around the source. Before proceeding to isolate the effects of each of these, we provide a qualitative description of the important physicochemical interactions taking place. Spagnolie *et al.* used solely hydrodynamics-based arguments to show that if the radius of a spherical obstacle is larger than a critical trapping radius, then it can hydrodynamically capture or trap swimmers that directly impinge upon it [see Fig. 2(a)]. Alternatively, swimmers with dipole strengths larger than a critical value can get hydrodynamically trapped around spherical obstacles [see Fig. 2(b)]. In addition, for all cases where hydrodynamic trapping is expected to occur, there exists a basin of attraction such that tangentially directed pusher swimmers that lie within the basin get trapped and travel along the surface of the sphere [see Fig. 2(c)]. The depth of this basin varies with the sphere radius $A$ and the dipole strength $\alpha_D$. It is at most 2.5 body lengths for $A$ as large as 200 and $\alpha_D = 0.8$. At such small separations, Molaei *et al.* have shown the inability of an *E. coli* cell to tumble or even escape the solid surface [22,71]. Therefore, hydrodynamics is strongest, and tumbling weakest, when the microorganism is located very close to the source. Conversely, when the microorganism is far from the source, the hydrodynamics becomes negligible and chemotaxis is the dominant factor in dictating its motion.

Thus, a bacterium located far away from the source can get attracted to and even trapped onto it via the following sequence of events: (i) chemotaxis, i.e., biased tumbling causing the bacterium to come within 2–3 body lengths from the source, followed by (ii) hydrodynamic attraction on account of the theory detailed in Secs. II A and II C. Once the bacterium reaches the nutrient, its behavior is governed by the interplay of (i) hydrodynamics, (ii) hard-core repulsion, and (iii) rotary diffusion. The interaction between the first two may result in the trapping of the microorganism, depending on its dipole strength and the radius of the source. If the radius is larger than the critical trapping radius (corresponding to the bacterium's dipole strength), then the bacterium will be trapped at the surface—due to a balance between hydrodynamic attraction and hard-core repulsion—and will orbit around the source. The third effect contributes to probable escape of any bacterium that would get trapped onto the surface based purely on hydrodynamics. The escape can occur due to a reorientation that turns the bacterium to an extent that $(\mathbf{u}_{HI} + V_s\mathbf{p}) \cdot \hat{\mathbf{r}} > 0$

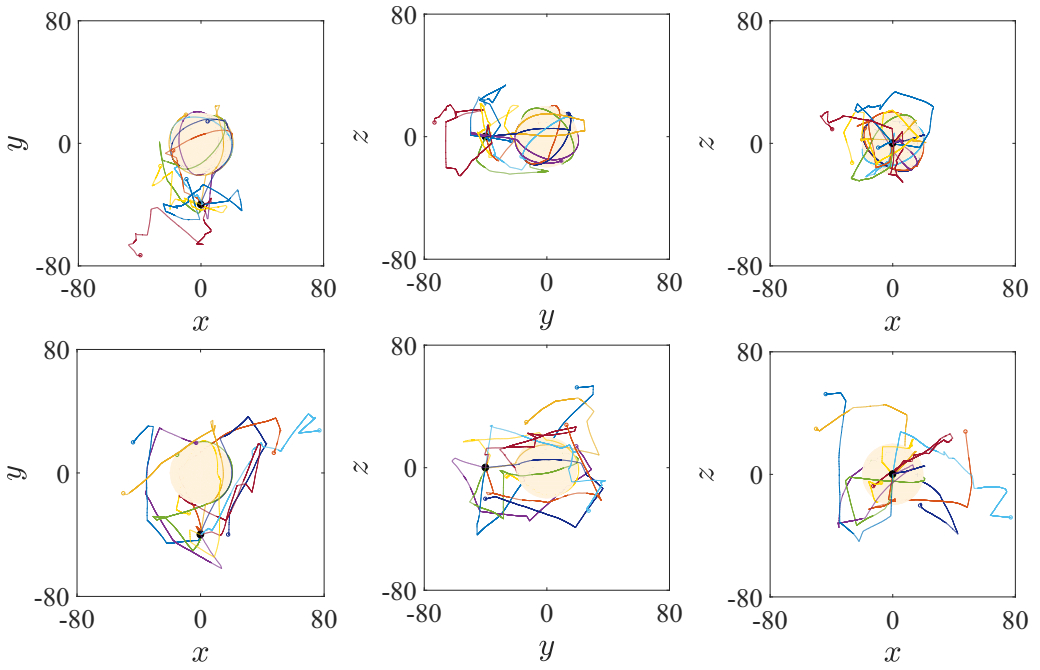


FIG. 4. A schematic of the effect of chemotaxis strength on the accumulation around the nutrient source. The left, central, and right columns show the $x$-$y$, $y$-$z$, and $x$-$z$ projections, respectively, of the microorganisms' trajectories. The microorganisms are located initially at $[x(0), y(0), z(0)] = [0, -40, 0]$, and oriented arbitrarily. It is important to note that in the absence of chemotaxis, most of the microorganisms would just swim away from the source without appreciably changing their orientations. The upper (resp. lower) row represents strong (resp. weak) chemotaxis, which could either be due to $C_0/K_D = 1.0$ (resp. $C_0/K_D \ll 1.0$), or a small (resp. large) value of $\tau^*$. Clearly, strong (resp. weak) chemotaxis leads to the microorganisms being, in general, closer to (resp. further from) the nutrient.

[see Eq. (17)], thus allowing it to swim away from the surface. This three-way coupling has been explained schematically in Fig. 3 and discussed in greater detail in Refs. [25,26]. Note also that rotary diffusion causing escape (for a variety of microorganisms) from solid surfaces has been observed experimentally in Refs. [20,21,42].

Quantitatively, it suffices to remember that hydrodynamic trapping is most favored for high values of $\alpha_D$ and low values of $D$. This is because large $\alpha_D$ results in stronger hydrodynamic attraction, and small $D$ reduces the influence of rotary diffusion. We further explain this idea in the next section. Table I summarizes the influence of the mechanisms discussed above, on the fate of a microorganism located initially at some arbitrary distance from the source and oriented along any arbitrary direction. Figure 4 shows typical trajectories and provides an understanding of microorganism distribution around the source for the case of strong and weak chemotaxis; in the subsequent sections, we quantify these results.

### B. Types of behaviors

Figure 5 provides us with an intuition about the different physical mechanisms dictating microorganism attraction and entrapment onto nutrient sources. It contains features of run-and-tumble chemotaxis as well as hydrodynamic trapping. We see that chemotaxis does not always succeed in bringing the microorganism to the source (red trajectory) or that chemotaxis can lead the microorganism close enough to the source but still outside its basin of attraction (blue trajectory). In the case shown by the magenta trajectory, we see how chemotaxis allows a microorganism to make contact with the source but it later gets scattered instead of being trapped. Finally, we also see how chemotaxis and hydrodynamics enable the microorganism to make contact with the source and then glide along its surface due to hydrodynamic entrapment (green trajectory). This rich variety of trajectories emerges due to an interplay involving varying strengths of one or all of the mechanisms

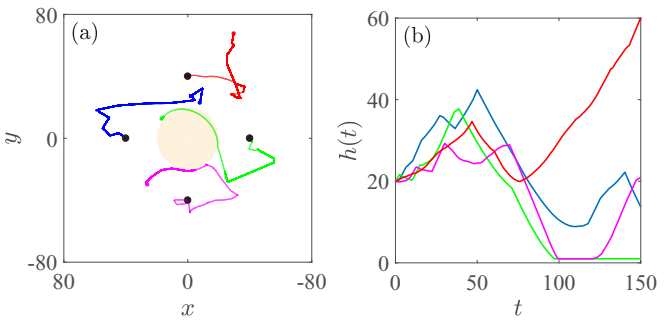


FIG. 5. (a) Visualization of the different behaviors elicited by the mechanisms discussed in Table I. The starting positions are shown by black dots. Red: this microorganism is unable to locate the source in the time for which the simulations were run. Blue: this microorganism chemotaxes close enough to the source, but does not enter the basin of hydrodynamic attraction. Magenta: in this case, the microorganism does make contact with the source, but the hydrodynamic attraction is not strong enough for trapping to occur. Green: an example of a successful trapping wherein chemotaxis and hydrodynamics work in conjunction to bring and trap a microorganism onto the source. See main text for details about the regimes in which such behaviors occur. (b) The time evolution of the distance from the source, $h(t)$, of trajectories in panel (a).

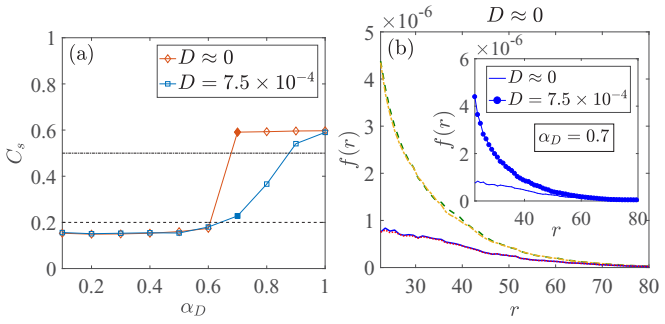


FIG. 6. (a) Variation of the surface concentration, $C_s$, with the dipole strength $\alpha_D$ for $D \approx 0$ (negligible rotary diffusion) and $D = 7.5\times10^{-4}$ (moderate rotary diffusion). (b) Main figure: The distribution $f(r)$ for $D \approx 0$, and $\alpha_D = 0.1$ (green dashed line), $\alpha_D = 0.6$ (orange dash-dotted line), $\alpha_D = 0.7$ (blue solid line), $\alpha_D = 1.0$ (red dotted line). Inset: The distribution $f(r)$ for $\alpha_D = 0.7$ for $D \approx 0$ and $7.5\times10^{-4}$ [corresponding surface concentrations are shown in panel (a) by filled symbols]. Notice the drastic difference in the values of $C_s$ and $f(r)$ for the two different values of rotary diffusivities.

detailed in Table I. It is clear that the phenomena being investigated is very nontrivial in all its complexity. A better understanding can be obtained by first considering limiting values of certain parameters and then moving on to more general parametric regimes. In particular, an understanding of the limiting scenarios $D \approx 0$ and/or $\alpha_D \approx 0$ is warranted. We will see that both these parameters play an important role in the extent of surface colonization $C_s$, and the nature of the distribution function $f(r)$.

### C. Influence of the dipole strength $\alpha_D$ and the rotary diffusivity $D$

Figure 6(a) shows the variation in $C_s$ with $\alpha_D$ for $D \approx 0$ and $D = 7.5\times10^{-4}$. The corresponding bulk distributions $f(r)$ are shown in Fig. 6(b). The other parameters are kept at their baseline values, such that chemotactic approach is guaranteed in most cases. The bulk concentration is highest near the surface and reduces monotonically to zero as $r$ increases. This shows that chemotaxis, on average, helps the microorganisms to locate nutrient-rich regions in their surroundings.

We note that for $D \approx 0$, the response is binary, i.e., $C_s$ is either $\approx$0.155 or $\approx$0.60 and $f(r)$ varies as one of the two discernible curves in the main plot of Fig. 6(b). This is because in the absence of orientational fluctuations, bacteria that enter the basin of attraction (through chemotaxis) behave deterministically: They either get trapped or they escape. For a given size of the source ($A = 20$ in all our results), the type of behavior—both qualitative *and* quantitative—depends only on the value of $\alpha_D$: (i) for large enough $\alpha_D$, a majority of microorganisms get trapped at $r \approx 20$, while (ii) for smaller $\alpha_D$, a majority is distributed in the bulk fluid [recall Fig. 2(b)]. This behavior can be understood by considering the dependence of hydrodynamic interactions on the dipole strength and on the distance of the microorganism from the source. At large distances, hydrodynamics has a negligible impact on reorienting the bacteria, and they behave more or less similarly, irrespective of their $\alpha_D$ values. However, once inside the basin, the fate of a bacterium (trap or escape) depends acutely on $\alpha_D$; and for a given size $A$, any bacterium with $\alpha_D$ above (resp. below) a critical value gets hydrodynamically trapped (resp. escapes). In fact, for a fixed $A$, purely hydrodynamics-based trapping occurs above a critical $\alpha_D \geqslant 8/(3A^{1/2})$ [25]. Therefore, for $A = 20$, trapping should occur for $\alpha_D \geqslant 0.65$, as evident in Fig. 6. Even then, the randomness of the initial approach means that $C_s < 1$; i.e., not all microorganisms get trapped (recall the red and the blue trajectories in Fig. 5).

Another feature of the results in this section is that higher $C_s$ values imply a lower average value of $f(r)$. This allows us to identify the regions where most of the microorganisms accumulate. In all scenarios when $C_s < 0.2$, the nature of $f(r)$ is such that $\int_A^{2A} 4\pi r^2 f(r) dr \approx 0.5$. This can be interpreted as an off-surface accumulation. It occurs due to an efficient chemotactic approach combined with weak hydrodynamic attraction, causing most microorganisms to gather within one (source) radius from the surface.

As a microorganism with $\alpha_D \geqslant 0.65$ comes in contact with the source, it begins to travel along the surface due to the mechanisms explained in Fig. 3. The only mechanism that can get such a trapped microorganism to escape is its own rotary diffusivity. This idea was explained schematically in Fig. 3 and an example of such an escape can be seen in the magenta trajectory of Fig. 5. Figure 6(a) shows (blue line marked with squares) the variation of $C_s$ with $\alpha_D$ for $D = 7.5\times10^{-4}$. It can be seen that rotary diffusivity markedly affects the tendency of the microorganism to accumulate at the surface and consequently, results in more microorganisms in the fluid surrounding the source [inset in Fig. 6(b)]. For example, for $\alpha_D = 0.7$ there is $\approx$60% reduction (resp. increment) in surface colonization (resp. average bulk distribution) for a modest rotary diffusivity. As the strength of hydrodynamic attraction grows ($\alpha_D$ increases), a greater fraction of the microorganisms get trapped at the surface, in spite of orientational fluctuations. Therefore, the near-field hydrodynamic attraction acts as a crucial mechanism that allows microorganisms to colonize nutrient sources.

Finally, whenever hydrodynamic attraction is weak ($\alpha_D < 0.65$), the rotary diffusivity does not affect the surface concentration at all (values of $C_s$ for $D \approx 0$ and $D > 0$ are coincident for $\alpha_D < 0.65$, for a wide range of $D$). This is understandable because if hydrodynamic interactions are weak, the microorganism just does not rotate fast enough to stay trapped onto the surface, and thus its escape is guaranteed regardless of other influences (see Fig. 3). The very weak dependence on $D$ comes from the fact that far away from the source—where the microorganisms predominantly reside—orientational changes due to rotary diffusivity are negligible as compared to those due to a tumble, as also seen for collective motion of active suspensions [72]. Figure 10 in the appendix shows that the bulk distributions are also practically identical in this case.

### D. Variability in chemotactic factors: $C_0/K_D$ and $\tau^*$

In Sec. III C, we saw the importance of hydrodynamics in trapping chemotactic microorganisms onto the source. We also explained how rotary diffusivity of the microorganisms reduces surface colonization. The main question that we aim to answer in this section is the following: How does chemotaxis-based

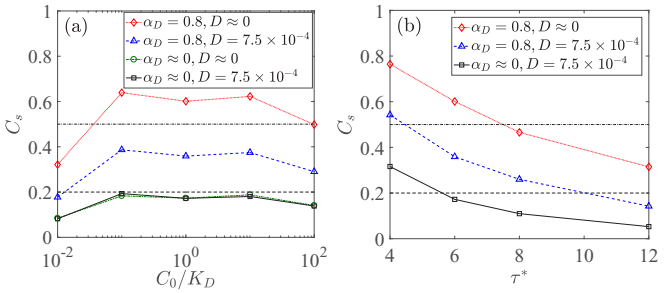


FIG. 7. Variation of the surface concentration $C_s$ with (a) $C_0/K_D$, and, (b) $\tau^*$. In each case, $C_s$ is highest when $\alpha_D > 0.65$ and $D$ is negligible, as expected based on the discussion in Sec. III C. Also, the results are independent of $D$ for $\alpha_D \approx 0$. For small $\tau^*$, $C_s$ varies almost linearly with $\tau^*$.

initial approach affect the colonization of nutrient sources by bacteria? There are two factors that we need to consider: (i) nutrient availability in the form of a prescribed background concentration and (ii) the microorganism's intrinsic response to gradients in nutrient concentration. The nutrient availability—which is an environmental factor—is quantified by the ratio $C_0/K_D$. Thus, it could be an indication of the actual concentration of a given chemoattractant at the source (e.g., the amount of soluble hydrocarbons in a drop of crude oil) or the affinity of the chemoreceptor to the chemoattractant [32]. The intrinsic chemotactic response—which is a motility trait of individual bacteria—depends on the mean tumbling frequency $\tau_0^{-1}$.

Does greater nutrient availability enhance the colonization of nutrient sources by bacteria? Figure 7(a) shows that this is not necessarily the case, irrespective of the hydrodynamic influences. The $C_s$ vs $C_0/K_D$ trend for all combinations (high/low) of $\alpha_D$ and $D$ is the same: an approximately twofold initial increase, followed by little change for a wide range of $C_0/K_D$, and then a reduction. There is not much difference in the surface concentration [and the bulk distribution; see Fig. 8(a)] between $C_0/K_D = 0.1, 1.0, 10.0$. This behavior is explained by the scaling of the run time $\tau$ with $C_0/K_D$, which can be easily assessed by examining Eq. (16). If $C_0 \ll K_D$, then $\tau/\tau_0 \sim \exp(DC/Dt)$; if $C_0 \sim K_D$, then $\tau/\tau_0 \sim \exp(C^{-1}DC/Dt)$; and if $C_0 \gg K_D$, then $\tau/\tau_0 \sim \exp(C^{-2}DC/Dt)$ [2]. This means that higher nutrient availability does not always result in a proportionate increase in the run time $\tau$ in nutrient-rich regions, and so it does not necessarily translate to improved chemotactic performance. In fact, if $C_0/K_D$ is increased even further to 100.0, then we observe a decline in $C_s$ as compared to the previous three cases, due to the dominant contribution of the $C^{-2}$ term, as described above. Physically, $C_0 \ll K_D$ would mean that the ambient nutrient concentration is not high enough to prompt rapid chemotaxis, while the other extreme $C_0 \gg K_D$ is equivalent to a nutrient abundance that makes chemotactic foraging unnecessary.

The chemotactic response of bacteria is much more sensitive to $\tau^*$ (dimensionless run time) than it is to $C_0/K_D$. The variation of $C_s$ with respect to $\tau^*$ is monotonic, and bacteria with lower mean run lengths are much more effective in colonizing nutrient sources. Figure 7(b) shows that surface

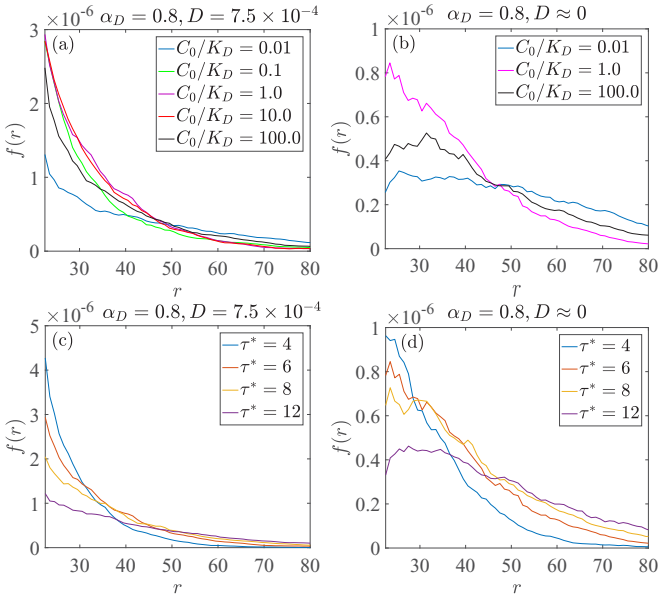


FIG. 8. The bulk distribution $f(r)$ as a function of [(a), (b)] $C_0/K_D$ and [(c), (d)] $\tau^*$. Note the almost similar distributions for $C_0/K_D = 0.1, 1.0, 10.0$, just like the corresponding $C_s$ values in Fig. 7. In conjunction with Fig. 7, it is evident how rotary diffusion causes more microorganisms to stay in the bulk. For weak chemotaxis, there is no appreciable accumulation anywhere in the bulk. $f(r)$ increases to a maximum and then decays to zero for weak chemotaxis in the panels (b) and (d). See main text for details.

colonization can be as high as 80% for $\tau^* = 4$. The green trajectory of Fig. 5 is a good example of such strong surface colonization, wherein chemotaxis enables the microorganism to make contact with the source and strong hydrodynamic attraction keeps it trapped at the surface. Owing to their random initial orientations, it is essential for the distant bacteria to tumble more frequently in order to locate the source. This is why bacteria with smaller $\tau^*$ values are able to orient themselves along $\nabla C$—and ultimately enter the basin of hydrodynamic attraction—faster than those with larger $\tau^*$, and high $C_s$ values for the former are just a consequence of this rapid chemotactic response.

An inspection of Fig. 8 in the context of Fig. 7 enables us to draw useful conclusions about the bacterial distribution in the bulk for different values of $C_0/K_D$ and $\tau^*$. A general observation from Fig. 7 is that chemotaxis can be considered strong (resp. weak) whenever $C_0/K_D \approx O(1)$ (resp. $C_0/K_D \ll 1$) and/or $\tau^* < 8$ (resp. $\tau^* > 8$). We see that the value of $f(r = 20)$ and the subsequent decline of $f(r)$ is much more gradual for weak chemotaxis [Figs. 8(a) and 8(c)], with $\int_A^{4A} 4\pi r^2 f(r) dr \approx 0.5$. This suggests insignificant accumulation at any particular location because the chemotactic bias is not strong enough. The curves for $C_0/K_D = 0.01, 100$ in Fig. 8(b) and for $\tau^* = 12$ in Fig. 8(d) exemplify the scenarios when hydrodynamic attraction is strong enough to promote surface aggregation, but the initial approach toward the source is highly hindered. As opposed to all other cases, these distributions exhibit a gentle maximum at a distance $r \approx 30$. This is an interesting aspect of the present study: the existence of a depletion zone in the bulk distribution of microorganism positions for all scenarios involving strong

hydrodynamics and weak chemotaxis. In spite of the latter effect, some microorganisms *do* encounter the source and get trapped onto it, while others move in an almost random fashion. The depletion zone spatially demarcates these two extremes.

## IV. CONCLUSION

We formulated a mathematical model and performed probabilistic simulations to ascertain the distribution of microorganisms around a spherical nutrient source. The model was based on, and the distribution was mediated by, a combination of (i) hydrodynamic interaction (HI) with the source and (ii) chemotaxis toward the nutrient or chemoeffector emanating from the source. In our model, we assumed that hydrodynamic interactions and rotary diffusion dominate in the near field of the nutrient source, while chemotaxis dominates when the microorganism is far away. This distinction stems from the fact that bacterial tumbling is hindered in the proximity of solid surfaces (thus precluding run-and-tumble chemotaxis and surface escape via tumbling) [22], and so near-surface bacterial behavior is governed by hydrodynamics in conjunction with rotary diffusion [20,21,25]. Hydrodynamic interactions can be strong or weak, depending on the value of the microorganism's dipole strength and the radius of the source. Chemotaxis too can be strong or weak, depending on the microorganism's mean tumbling frequency and the nutrient availability in its surroundings. Therefore, the distribution is affected by environmental (source size and nutrient availability) factors, as well as by the microorganism's intrinsic motility features (dipole strength, tumbling frequency, etc.). Although both hydrodynamics and chemotaxis attract a bacterium toward the source, their separate domains of influence and relative strengths can lead to interesting changes in the spatial distribution of microorganisms around the surface from which the nutrient diffuses out into the environment. To this end, we performed a systematic parametric study and revealed different surface colonization and bulk distribution features, highlighted in Fig. 9.

We see that stronger HI always leads to greater surface colonization (i.e., the quantity $C_s$), irrespective of the strength of the chemotactic influence. Similarly, stronger chemotaxis always leads to greater surface colonization, irrespective of the strength of the hydrodynamic influence. Understandably, $C_s$ is greatest when both the influences are strong, because this scenario corresponds to a more effective initial approach (toward the source) due to chemotaxis, followed by a strong hydrodynamic attraction. On the other hand, it is the least when both chemotaxis and HI are weak. The surface colonization is also not substantial ($C_s < 0.5$) whenever chemotaxis or HI is weak. Strong chemotaxis but weak HI leads to an off-surface accumulation with majority of microorganisms collecting in the bulk within a distance of one (source) radius from the surface. Finally, we find an interesting bulk distribution for the case of weak chemotaxis and strong HI, which leads to the formation of a depletion zone in the microorganism distribution, characterized by a gentle maximum in the value of $f(r)$ at $r \approx 30$. This is because weak chemotaxis does not enable enough bacteria to come close to the source, but those that do come close enough get trapped due to strong hydrodynamic attraction. These sufficiently general trends help establish the importance of chemotaxis and hydrodynamics in our problem. From them, we conclude that strong chemotaxis is essential to obtain greater aggregation of microorganisms near nutrient sources, and strong hydrodynamic interactions enable surface colonization. In addition to these generalities, we also find that higher nutrient availability—reflected in the value of the dimensionless parameter $C_0/K_D$—does not lead to proportionate increase in surface colonization [see Fig. 7(a)]. This is because the bacterium's run length $\tau$ depends on both its ambient nutrient concentration, $C$, and the instantaneous rate at which this concentration changes, $DC/Dt$, via Eq. (16). However, strong chemotaxis on account of lesser mean run time $\tau_0$ is much more effective in enhancing the surface colonization [see Fig. 7(b)]. In this way, our study yields a qualitative and quantitative insight into the process of bacterial attraction to, and aggregation around, nutrient sources under the combined influence of the two major factors dictating microorganism locomotion: passive response via hydrodynamics and active response via chemotaxis.

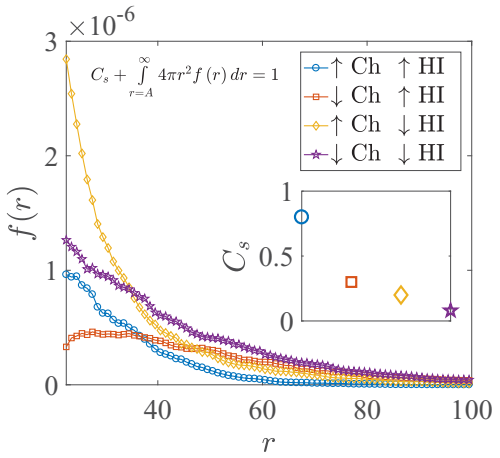


FIG. 9. The four qualitatively different behaviors, or spatial distributions $f(r)$, that can be realized due to the combined influence of hydrodynamics (abbreviated in the legend as HI) and chemotaxis (abbreviated in the legend as Ch) on the locomotion of microorganisms around a spherical nutrient source. ↑ (resp. ↓) denotes a strong (resp. weak) influence. The inset shows the surface colonization $C_s$ for each of the four behaviors, with correspondence based on marker type.

An important assumption in our study is that tumbling, and hence chemotaxis, is suppressed when the bacterium is at a distance less than or equal to two body lengths from the source. The basis of this assumption is the experimental work by Molaei *et al.* which confirmed tumbling suppression near rigid walls [22,71]. In addition, we use the model proposed by Brown and Berg to incorporate bacterial chemotaxis [2] and neglect any "memory effects" when calculating the run time in the presence of a chemoeffector [see Eq. (16)]. We emphasize that the finer aspects of chemotaxis can be easily incorporated into our study, like tumbling anisotropy enforced due to proximity to surfaces and/or due to altogether different foraging tactics like reversals and flicks. It would be interesting to see the extent to which these influences affect the results of our study. Equally interesting is the possibility of studying hydrodynamic interactions between microorganisms in the semidilute regime and

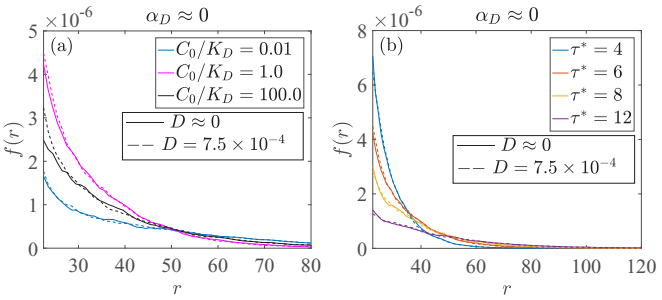


FIG. 10. The bulk distribution $f(r)$ as a function of (a) $C_0/K_D$ and (b) $\tau^*$ for negligibly small hydrodynamic attraction ($\alpha_D \approx 0$) and $D \approx 0$, $D = 7.5\times10^{-4}$.

how it would affect their spatial distribution around nutrient sources. A more complex mathematical model—one which includes some, or all, of the aforementioned effects—would require experiments to ascertain tumbling alteration close to curved surfaces and predict bacterial re-orientations differing from the archetypal tumble. The present study improves our understanding of bacterial colonization of surfaces and is expected to have far-reaching consequences in bioremediation, selective microorganism capture, lab-on-a-chip assays and investigations on bacteria in porous media.

Data are publicly available through the Gulf of Mexico Research Initiative Information and Data Cooperative (GRIIDC) [73].

## ACKNOWLEDGMENTS

This research was made possible by grants from the Gulf of Mexico Research Initiative and the NSF, CBET-1700961 and CBET-1705371. The authors thank Roseanne M. Ford for useful discussions. N.D. would like to thank Aditya Bandopadhyay for useful discussions. The authors also thank the anonymous referees for their suggestions in improving the quality of this paper.

## APPENDIX

In Fig. 7, we saw that rotary diffusivity has no effect on the surface colonization when hydrodynamic effects are negligible, i.e., $\alpha_D \approx 0$. Figure 10 shows that even the bulk distribution is not affected significantly in this case. This is because for $\alpha_D \approx 0$, the microorganisms execute a biased random walk and get reflected from the surface irrespective of the magnitude of rotary diffusion, as explained in Sec. III C.

In Sec. II B, we mentioned that the effect of rotary diffusion as given by Eq. (8) is strictly correct only if the rotary diffusion tensor—say $\mathbf{D_R}$—is isotropic, i.e., when $\mathbf{D_R} = D_r\mathbf{I}$. In reality, the presence of a surface and the approach of bacterium to the spherical source imparts anisotropy and time dependence, respectively, to $\mathbf{D_R}$. The stochastic effects become considerably involved when the diffusivities evolve with time (see Eqs. (13) and (14) in Ref. [56]). However, in our problem, fluctuations in the bacterial orientation are only important in the near field, i.e., when a bacterium orbits around the source [see Fig. 3, Table I, and the discussion in the last paragraph

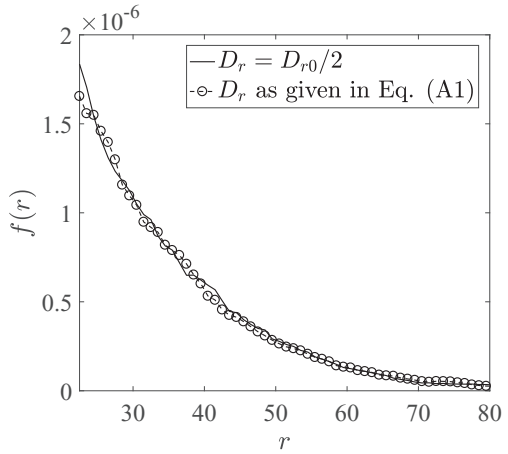


FIG. 11. The bulk distribution $f(r)$ for two different cases: (i) when the value of $D_r$ in Eq. (8) is taken to be half of the rotary diffusivity in an unbounded fluid, $D_{r0}$, in the *entire* domain (solid line) and (ii) when Eq. (A1) is used to assign bacterial rotary diffusivities based on separation of the microorganism from the source (dashed line marked with circles). The surface colonization values are within 1.25% of each other. The value of the dimensionless rotary diffusivity in unbounded fluid is $7.5\times10^{-4}$, i.e., $D_{r0}b/V_s = 7.5\times10^{-4}$.

of Sec. III C in relation to Figs. 6(a) and 10]. Also, the change in $\|\mathbf{D_R}\|$ for a sphere is most significant when it is very close to a solid wall [74–76]. In fact, using the mobility expressions given by Cichocki and Jones [75] we can estimate that $\|\mathbf{D_R}\|$ is halved when a sphere almost makes contact with the wall (assuming, of course, that their results can be reasonably used for our configuration of two spheres—the source and the bacterium—because $R/b \gg 1$). Therefore, the $D_r$ in Eq. (8) can be considered as the reduced rotary diffusivity due to close

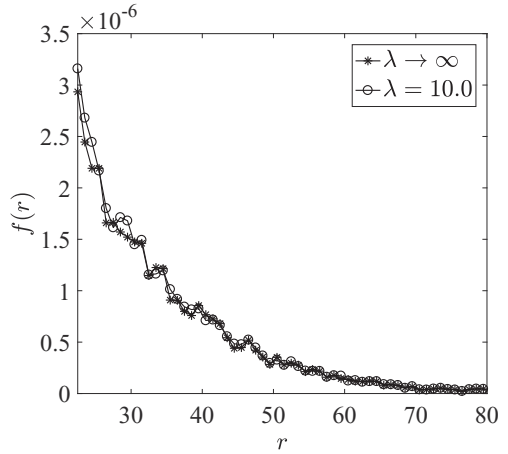


FIG. 12. Comparison of the bulk distribution $f(r)$ for combined chemotactic and hydrodynamic attraction to (i) a rigid sphere (asterisks) and (ii) a clean drop with viscosity ratio $\lambda = 10$ corresponding to crude oil (circles), for the baseline simulation parameters given in Sec. III A. The difference between the two cases is not very significant. The surface colonization for the rigid sphere ($C_{s,\text{rigid}} = 0.3589$) is 4% larger than that for the drop ($C_{s,\text{drop}} = 0.3446$). For motion around the drop, the hydrodynamics-induced linear and angular velocities are taken from Ref. [48].

proximity to a surface. In other words, if the rotary diffusivity in the unbounded fluid is $D_{r0}$, then that near the source will be $D_r = kD_{r0}$, where $k \approx 1/2$. Note that using two different values of $D_r$,

$$D_r = \begin{cases} D_{r0}, & |\mathbf{x}_2| \gg (R+b) \\ \frac{D_{r0}}{2}, & |\mathbf{x}_2| \approx (R+b) \end{cases}, \tag{A1}$$

instead of using only $D_r = (D_{r0}/2)$ everywhere in the domain, will not change our results appreciably, once again because of the near-field significance of rotary diffusion (see Fig. 11).

The methodology outlined in Sec. II also enables us to compute the distribution of microorganisms around more general surfaces, for example, that near fluid-fluid interfaces. The fundamental difference in this case is that the boundary conditions change from those given in Eq. (3), to the more general form of continuity of fluid velocity and stress [43]. As a result, for microorganism motion around clean drops, the viscosity ratio of the drop with respect to the suspending fluid—denoted by $\lambda$—appears as an extra parameter that can dictate the distribution function $f(r)$. This change is reflected in the expressions for $\mathbf{u}_{HI}$ and $\boldsymbol{\Omega}_{HI}$, which were derived recently by Shaik and Ardekani [48]. If we assume that the near-field hydrodynamic and tumbling characteristics remain the same as those in Sec. II C and that the microorganism does not simply adsorb onto the drop's surface, we can estimate the distribution of chemotactic bacteria around drops as well. Figure 12 shows the spatial distribution of chemotactic microorganisms around a stationary drop with viscosity ratio 10, which is indicative of crude oil [77]. The distribution is almost the same as that around a rigid, spherical nutrient source (limiting case of $\lambda \to \infty$), thus suggesting the utility of our results in the analysis of biodegradation of hydrocarbon effusing crude oil drops.


[1] H. C. Berg and D. A. Brown, Nature (London) **239**, 500 (1972).
[2] D. A. Brown and H. C. Berg, Proc. Natl. Acad. Sci. USA **71**, 1388 (1974).
[3] H. C. Berg, *Random Walks in Biology*, 2nd ed. (Princeton University Press, Princeton, NJ, 1993).
[4] H. C. Berg, *E. coli in Motion* (Springer-Verlag, New York, 2004).
[5] M. Eisenbach, J. Lengeler, M. Varon, D. Gutnick, R. Meili, R. Firtel, J. Segall, G. Omann, A. Tamada, and F. Murakami, *Chemotaxis* (Imperial College Press, London, 2004).
[6] H. Szurmant and G. W. Ordal, Microbiol. Mol. Biol. Rev. **68**, 301 (2004).
[7] G. H. Wadhams and J. P. Armitage, Nat. Rev. Mol. Cell Biol. **5**, 1024 (2004).
[8] R. Lux and W. Shi, Crit. Rev. Oral Biol. Med. **15**, 207 (2004).
[9] S. L. Porter, G. H. Wadhams, and J. P. Armitage, Nat. Rev. Microbiol. **9**, 153 (2011).
[10] R. Stocker, Proc. Natl. Acad. Sci. USA **108**, 2635 (2011).
[11] E. Lauga and T. R. Powers, Rep. Prog. Phys. **72**, 096601 (2009).
[12] W. R. DiLuzio, L. Turner, M. Mayer, P. Garstecki, D. B. Weibel, H. C. Berg, and G. M. Whitesides, Nature (London) **435**, 1271 (2005).
[13] E. Lauga, W. R. DiLuzio, G. M. Whitesides, and H. A. Stone, Biophys. J. **90**, 400 (2006).
[14] L. Lemelle, J.-F. Palierne, E. Chatre, and C. Place, J. Bacteriol. **192**, 6307 (2010).
[15] R. Di Leonardo, D. Dell'Arciprete, L. Angelani, and V. Iebba, Phys. Rev. Lett. **106**, 038101 (2011).
[16] M. Morse, A. Huang, G. Li, M. R. Maxey, and J. X. Tang, Biophys. J. **105**, 21 (2013).
[17] K. Ishimoto and E. A. Gaffney, Phys. Rev. E **88**, 062702 (2013).
[18] L. Cisneros, C. Dombrowski, R. E. Goldstein, and J. O. Kessler, Phys. Rev. E **73**, 030901 (2006).
[19] A. P. Berke, L. Turner, H. C. Berg, and E. Lauga, Phys. Rev. Lett. **101**, 038102 (2008).
[20] G. Li and J. X. Tang, Phys. Rev. Lett. **103**, 078101 (2009).
[21] G. Li, J. Bensson, L. Nisimova, D. Munger, P. Mahautmr, J. X. Tang, M. R. Maxey, and Y. V. Brun, Phys. Rev. E **84**, 041932 (2011).
[22] M. Molaei, M. Barry, R. Stocker, and J. Sheng, Phys. Rev. Lett. **113**, 068103 (2014).
[23] K. Schaar, A. Zöttl, and H. Stark, Phys. Rev. Lett. **115**, 038101 (2015).
[24] S. E. Spagnolie and E. Lauga, J. Fluid Mech. **700**, 105 (2012).
[25] S. E. Spagnolie, G. R. Moreno-Flores, D. Bartolo, and E. Lauga, Soft Matter **11**, 3396 (2015).
[26] N. Desai, V. Shaik, and A. M. Ardekani, Soft Matter **14**, 264 (2018).
[27] G. O'Toole, H. B. Kaplan, and R. Kolter, Annu. Rev. Microbiol. **54**, 49 (2000).
[28] T. Danhorn and C. Fuqua, Annu. Rev. Microbiol. **61**, 401 (2007).
[29] A. Karimi, D. Karig, A. Kumar, and A. M. Ardekani, Lab Chip **15**, 23 (2015).
[30] G. A. Jackson, Limnol. Oceanogr. **32**, 1253 (1987).
[31] G. A. Jackson, Limnol. Oceanogr. **34**, 514 (1989).
[32] R. Bearon and T. J. Pedley, Bull. Math. Biol. **62**, 775 (2000).
[33] T. Kiørboe and G. A. Jackson, Limnol. Oceanogr. **46**, 1309 (2001).
[34] T. Kiorboe, H.-P. Grossart, H. Ploug, and K. Tang, Appl. Environ. Microbiol. **68**, 3996 (2002).
[35] R. N. Bearon, Bull. Math. Biol. **69**, 417 (2007).
[36] J. T. Locsei and T. J. Pedley, Microb. Ecol. **58**, 63 (2009).
[37] R. Stocker, Science **338**, 628 (2012).
[38] R. Stocker and J. R. Seymour, Microbiol. Mol. Biol. Rev. **76**, 792 (2012).
[39] E. Lushi, R. E. Goldstein, and M. J. Shelley, Phys. Rev. E **86**, 040902 (2012).
[40] E. Lushi, Phys. Rev. E **94**, 022414 (2016).
[41] D. Takagi, J. Palacci, A. B. Braunschweig, M. J. Shelley, and J. Zhang, Soft Matter **10**, 1784 (2014).
[42] K. Drescher, J. Dunkel, L. H. Cisneros, S. Ganguly, and R. E. Goldstein, Proc. Natl. Acad. Sci. USA **108**, 10940 (2011).
[43] L. G. Leal, *Advanced Transport Phenomena* (Cambridge University Press, Cambridge, UK, 2007).
[44] G. M. Barbara and J. G. Mitchell, FEMS Microbiol. Ecol. **44**, 79 (2003).

[45] D. Lopez and E. Lauga, Phys. Fluids **26**, 071902 (2014).
[46] V. A. Shaik and A. M. Ardekani, J. Fluid Mech. **824**, 42 (2017).
[47] S. Kim and S. Karrila, *Microhydrodynamics: Principles and Selected Applications* (Butterworth- Heinemann, Boston, 1991).
[48] V. A. Shaik and A. M. Ardekani, Phys. Rev. Fluids **2**, 113606 (2017).
[49] I. M. Head, D. M. Jones, and W. F. M. Röling, Nat. Rev. Microbiol. **4**, 173 (2006).
[50] L. Turner, W. S. Ryu, and H. C. Berg, J. Bacteriol. **182**, 2793 (2000).
[51] M. J. Kim, M. J. Kim, J. C. Bird, J. Park, T. R. Powers, and K. S. Breuer, Exp. Fluids **37**, 782 (2004).
[52] N. C. Darnton and H. C. Berg, Biophys. J. **92**, 2230 (2007).
[53] J. Elgeti, R. G. Winkler, and G. Gompper, Rep. Prog. Phys. **78**, 056601 (2015).
[54] C. Bechinger, R. Di Leonardo, H. Löwen, C. Reichhardt, G. Volpe, and G. Volpe, Rev. Mod. Phys. **88**, 045006 (2016).
[55] P. D. Cobb and J. E. Butler, J. Chem. Phys. **123**, 054908 (2005).
[56] M. De Corato, F. Greco, G. D'Avino, and P. L. Maffettone, J. Chem. Phys. **142**, 194901 (2015).
[57] P. D. Frymier, R. M. Ford, and P. T. Cummings, AIChE J. **40**, 704 (1994).
[58] K. Duffy, P. Cummings, and R. Ford, Biophys. J. **68**, 800 (1995).
[59] M. Abramowitz and I. A. Stegun, *Handbook of Mathematical Functions with Formulas, Graphs, and Mathematical Tables* 9th ed. (Dover, New York, 1972).
[60] K. C. Chen, R. M. Ford, and P. T. Cummings, J. Math. Biol. **47**, 518 (2003).
[61] D. Saintillan, Annu. Rev. Fluid Mech. **50**, 563 (2018).
[62] P. J. Brandvik, Ø. Johansen, F. Leirvik, U. Farooq, and P. S. Daling, Mar. Pollut. Bull. **73**, 319 (2013).
[63] Ø. Johansen, P. J. Brandvik, and U. Farooq, Mar. Pollut. Bull. **73**, 327 (2013).
[64] E. W. North, E. E. Adams, A. E. Thessen, Z. Schlag, R. He, S. A. Socolofsky, S. M. Masutani, and S. D. Peckham, Environ. Res. Lett. **10**, 024016 (2015).
[65] E. L. Cussler, *Diffusion: Mass Transfer in Fluid Systems*, 2nd ed. (Cambridge University Press, New York, 1997).
[66] G. A. Jackson, J. Exp. Biol. **215**, 1017 (2012).
[67] R. C. Macnab and D. E. Koshland Jr., Proc. Natl. Acad. Sci. USA **69**, 2509 (1972).
[68] E. A. Codling, M. J. Plank, and S. Benhamou, J. R. Soc., Interface **5**, 813 (2008).
[69] M. J. Tindall, S. L. Porter, P. K. Maini, G. Gaglia, and J. P. Armitage, Bull. Math. Biol. **70**, 1525 (2008).
[70] K. Son, F. Menolascina, and R. Stocker, Proc. Natl. Acad. Sci. USA **113**, 8624 (2016).
[71] M. Molaei and J. Sheng, Sci. Rep. **6**, 35290 (2016).
[72] G. Subramanian, D. L. Koch, and S. R. Fitzgibbon, Phys. Fluids **23**, 041901 (2011).
[73] N. Desai and A. Ardekani, Data for "Combined influence of hydrodynamics and chemotaxis in the distribution of microorganisms around spherical nutrient sources," https://doi.org/10.7266/N7GQ6W92 (2018).
[74] G. Perkins and R. Jones, Phys. A (Amsterdam, Neth.) **189**, 447 (1992).
[75] B. Cichocki and R. Jones, Phys. A (Amsterdam, Neth.) **258**, 273 (1998).
[76] R. B. Jones, J. Chem. Phys. **123**, 164705 (2005).
[77] J. M. Al-Besharah, O. A. Salman, and S. A. Akashah, Ind. Eng. Chem. Res. **26**, 2445 (1987).

*Correction:* The data availability statement has now been anchored with complete source information.